Unsupervised, fast and efficient colour-image copy protection

A. Abadpour and S. Kasaei

Abstract: The ubiquity of broadband digital communications and mass storage in modern society has stimulated the widespread acceptance of digital media. However, easy access to royalty-free digital media has also resulted in a reduced perception in society of the intellectual value of digital media and has promoted unauthorised duplication practices. To detect and discourage the unauthorised duplication of media, researchers have investigated watermarking methods to embed ownership data into media. However, some authorities have expressed doubt over the efficacy of watermarking methods to protect digital media. The paper introduces a novel method to discourage unauthorised duplication of digital images by introducing reversible, deliberate distortions to the original image. The resultant image preserves the image size and essential content with distortions in edge and colour appearance. The proposal method also provides an efficient reconstruction process using a compact key to reconstruct the original image from the distorted image. Experimental results indicate that the proposed method can achieve effective robustness towards attacks, while its computational cost and quality of results are completely practical.

1 Introduction

The Internet provides an entertainment and informational resource, rich with audio, images and video. While much of the resources on the Internet are recognised as 'free', the modern Internet is also a market for businesses supplying and distributing their digital media. With recent developments and price-positioning in digital media equipment, the Internet provides an ideal medium for the distribution of digital media. However, the same developments in broadband communications and mass storage hardware also provide opportunities for the unauthorised duplication and distribution of digital media. The reasons which make the Internet so persuasive as a distribution medium are also the concern when protecting intellectual property.

Over the last decade, much research has concentrated on the protection of digital media against unauthorised duplication and distribution [1]. The most recognised method in the field is watermarking [2]. In the watermarking method, authorisation data are added to the original data to help to identify the owner. Over the last decade, many interesting and original methods have been proposed for adding watermarks to digital media [3–15]. Unfortunately, equally interesting and original methods have been proposed for circumventing the protection offered by these watermarking methods. In fact, the equal development of cheating methods makes it undoubtable that, for any watermarking method, there are generally affordable methods of attack to corrupt the watermark or embed another watermark [16]. The robustness of different watermarking methods against attack has been considered by many researchers [17–20]. Table 1 compares a few typical watermarking methods in terms of attack resistance. A survey on security scenarios in music watermarking and their failure has been published [21]. The competing sides of watermarking technologies have prompted NASA experts to publish guidelines for image protection methods, with a statement advising to 'never expose an image in its large size', and suggesting to use 'visual watermarks' and 'programming shields' [22].

Recently, the efficacy of watermarking methods has been criticised by senior members of the image-processing community [23]. After Herley's controversial note on watermarking, entitled 'Why watermarking is nonsense' [23], researchers have emphasised that this immature field of signal processing is 'oversold' and that no method has yet been able to claim 'the ability to protect from all possible future attacks' [24, 25]. M. Barni comments, 'Why should we hide the information within the data, when we could more easily use headers or other means to reach the same good?' [26].

In response to public criticism, watermark researchers currently emphasise applications with less-restrictive requirements and look forward to emerging techniques to solve the fundamental problems [25]. In a very different approach, a few researchers have worked on direct copy detection [27], but it is also not yet a stable practical tool.

Of all digital media, digital image hardware have seen the greatest technological developments over recent years. The costs of consumer and professional digital camera equipment and duplication hardware have improved to the point where digital images are considered comparable with traditional film. The distribution and protection of commercial digital images presents additional requirements to copy protection methods. This paper considers methods for protecting digital images.

IEE Proceedings online no. 20050028

doi:10.1049/ip-com:20050028

Paper first received 25th January 2005 and in final revised form 5th May 2005

A. Abadpour is a master student in the Mathematics Science Department, Sharif University of Technology, Azadi Ave., Tehran, Iran

S. Kasaei is with the Computer Engineering Department, Sharif University of Technology, Azadi Ave., PO Box 11365-9517, Tehran, Iran

E-mail: skasaei@sharif.edu

Table 1: Attack resistance performance of some typical watermarking methods (adopted from [42])

Method		[2]	[46]	[47]	[5]	[4]	[48]	[49]	[50]	[51]	[52]	[6]
Attack type	LG	~	✓	~	~	~	✓		✓	✓	~	~
	NLG											
	LPO				~							
	NLPO		~	~	~	~	~		~			~
	SO		~	~	~	~	~		~	~	~	~
	EO											
	CMP	✓	✓	✓	✓	✓	✓	~	✓	✓	✓	✓

Not resistant; ~ Marginally resistant; ✓ Completely resistant; LG = linear geometrical transformation; NLG = nonlinear geometrical transformation; LPO = linear point operations; NLPO = nonlinear point operations; SO = spatial domain operations; EO = editiing operations; CMP = JPEG compression

The traditional practice for the distribution of commercial images involves sending down-sampled, cropped or visually-watermarked images for customer evaluation. When the customer chooses to purchase the images, the original, high-quality images are provided to replace the evaluation images. In this approach, the discarded information available in the evaluation images and the bandwidth consumed in acquiring these images is wasted. This paper proposes a method which permits the original images to be regenerated using a small-sized key, and ultimately results in improved bandwidth efficiency.

The evaluation images are intentionally manipulated to maintain the visual content, while containing many fake edges and colour alterations to make it inappropriate for unauthorised professional distribution. The original images are registered with the application of a small-sized key. The primary benefit of the proposed method is that the original image is efficiently reconstructed in a lossless framework.

The proposed method manipulates regions on homogeneous image texture for a protection against unauthorised duplication and distribution and extends the method of principal component analysis (PCA) [28]. Processing methods derived from the PCA technique have been shown to exhibit improved classification in colour images compared to well-known techniques such as the fuzzy C-means (FCM) [29]. Previous work has also developed a fast PCA-based colour transfer method to recolour an image using the colour information extracted from a reference image [30].

The proposed method assumes colour images as vector geometries and applies vectorial tools on them. This approach contrasts with the general approach of considering colour images as a set of parallel gray-scale images or using standard colour spaces [31–33]. A technique for describing homogeneous textures within an image based on PCA called linear partial reconstruction error (LPRE) has been proven to be a powerful representation [34]. The LPRE algorithm has been used as the basis of an algorithm called fuzzy principal component analysis-based clustering (FP-CAC), for the classification of image texture and has proved its superiority over the commonly used Euclidean and Mahalanobis likelihood distance-based approaches [35, 36].

The following Section discusses the proper likelihood measurement function for colour fields and briefly reviews the fuzzy companion of the PCA (called FPCA). The FPCA algorithm is used in a clustering method called FPCAC and introduces a PCA-based recolouring method and incorporates the different approaches in the proposed colour-image copy-protection algorithm.

2 Proposed method

In this Section, we first review some preliminary concepts of PCA-based analysis of colour images, the classification of homogeneous colour regions and the efficient representation of homogeneous textures.

2.1 PCA-based colour image processing

PCA considers a colour image as vector geometries and applies vectorial tools on them.

When attempting to analyse random variables of dimensions more than unity, there are several choices for the vector-to-set metric. A careless selection in this stage can decline the performance of the subsequent stages. The classic distance functions, such as Euclidean and Mahalanobis, are frequently used in available approaches, but recent research has shown that neither of them can be considered as the optimal choice for all physical phenomena.

It is mathematically proven [37], and empirically shown by experiment [34, 36], that the best available distance function for the sets of three-dimensional (3D) colour vectors the *RGB* colour space is the linear partial reconstruction error (LPRE) define as

$$\tau(\mathbf{c}, \boldsymbol{C}) = \left\|(\mathbf{c} - \boldsymbol{\eta}_C) - \mathbf{v}_C^T(\mathbf{c} - \boldsymbol{\eta}_C)\mathbf{v}_C\right\|^2 \qquad (1)$$

in which $\boldsymbol{C}$ is the set of colour vectors $\mathbf{c}$ is a single colour realisation. Also, $\boldsymbol{\eta}_C$ and $\mathbf{v}_C$ are the expectation vector and the first principal direction of $\boldsymbol{C}$, respectively.

Here, we give an illustrative example for comparing the performance of the LPRE-based query extraction in colour images with the results of the same operation applied when using the Euclidean and Mahalanobis-based distances (see Fig. 1). Query region extraction is the process of finding the region similar to a given query. Note the superiority of the LPRE-based approach compared with the two other distances in Fig. 1. Interested readers can find more examples of LPRE-based query region extraction in [38]. Also, see [35, 36] for the performance comparison of the LPRE with the Euclidean and Mahalanobis distances for other image-processing applications.

2.2 Fuzzy principal component analysis (FPCA)

Consider the problem of finding the principal components of the fuzzy set $\tilde{\boldsymbol{X}} = \{(\mathbf{x}_i; p_i) | i = 1, \ldots, n\}$. It

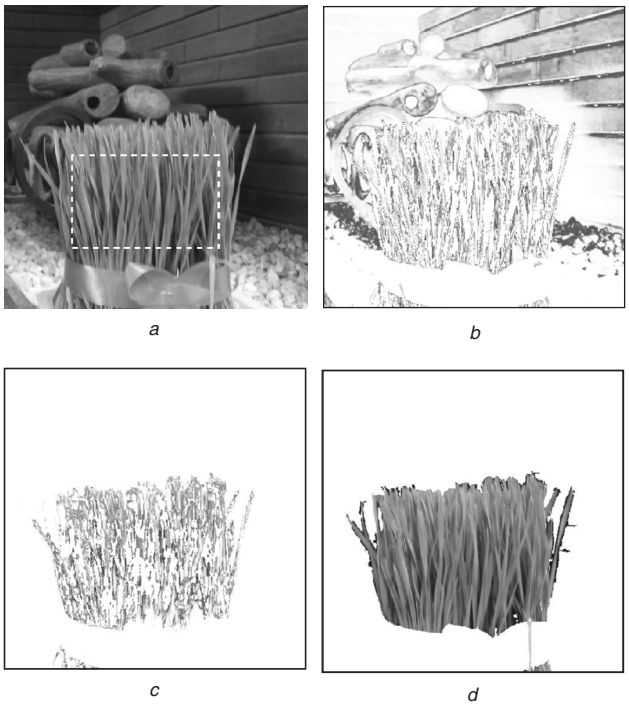

Fig. 1 *Query region extraction using different distance functions*
a Original image
b Euclidean
c Mahalanobis
d LPRE

is proved in [35] that computing the fuzzy expectation vector as

$$\boldsymbol{\eta}_{\tilde{X}} = \frac{1}{\sum_{i=1}^{n} p_i} \sum_{i=1}^{n} p_i \mathbf{x}_i \tag{2}$$

and the fuzzy covariance matrix as

$$\boldsymbol{C}_{\tilde{X}} = \frac{1}{\sum_{i=1}^{n} p_i} \sum_{i=1}^{n} p_i (\mathbf{x}_i - \boldsymbol{\eta}_{\tilde{X}})^T (\mathbf{x}_i - \boldsymbol{\eta}_{\tilde{X}}) \tag{3}$$

yields a perfect dual of PCA for fuzzy sets. In this way, the fuzzy principal directions of $\tilde{\boldsymbol{X}}$ are the eigenvectors of $\boldsymbol{C}_{\tilde{X}}$ sorted by the corresponding eigenvalues in an ascending fashion. Also, the PCA matrix of $\tilde{\boldsymbol{X}}$ comes from the singular value decomposition (SVD) of $\boldsymbol{C}_{\tilde{X}}$.

2.3 Fuzzy principal-component-based clustering (FPCAC) of colour vectors

Consider the general clustering problem stated as minimising the objective function defined as

$$\boldsymbol{J}(\boldsymbol{X}, \boldsymbol{\Phi}) = \sum_{i=1}^{n} \sum_{j=1}^{C} p_{ij}^m D_{ij} \tag{4}$$

This problem describes the best choice for clustering the members of the set $\boldsymbol{X} = \{\mathbf{x}_1, \ldots, \mathbf{x}_n\}$ into $\boldsymbol{C}$ clusters described as $\boldsymbol{\Phi} = \{\phi_1, \ldots, \phi_C\}$. Here, p_{ij} is the fuzzy membership of $\mathbf{x}_i$ to the jth cluster and D_{ij} is the distance from $\mathbf{x}_i$ to the jth cluster. Here, $m > 1$ is the fuzziness parameter. Assume that $D_{ij} = \Psi(\mathbf{x}_i, \boldsymbol{\phi}_j)$ is the appropriate distance function for the vector geometry under investigation. As an example, as discussed in Section 2.1, the LPRE is the proper distance for colour vectors. Here, ϕ_j is the defining parameter of the jth cluster, according to the general cluster model. Again, as an example in the LPRE methodology, $\boldsymbol{\phi}_j = [\boldsymbol{\eta}_j, \mathbf{v}_j]$.

Assume that the function Υ tunes the cluster model ϕ_j to best fit a fuzzy set of vectors. This means that, for the fuzzy set of vectors $\tilde{\boldsymbol{X}} = \{(\mathbf{x}_i; p_i) | i = 1, \ldots, n\}$,

$$\Upsilon(\tilde{\boldsymbol{X}}) = \arg_{\phi} \min \left\{ \sum_{i=1}^{n} p_i \Psi(\mathbf{x}_i, \phi) \right\} \tag{5}$$

Therefore, the function $\Upsilon(\tilde{\boldsymbol{X}}) \equiv \tilde{E}(\tilde{\boldsymbol{X}})$ is the companion for $\Psi(\mathbf{x}, \phi) = \|\mathbf{x} - \boldsymbol{\eta}\|^2$. Here, $\tilde{E}\{\tilde{\boldsymbol{X}}\}$ stands for the fuzzy expectation of a fuzzy set. Also, the FPCA introduced in Section 2.2 gives the $\Upsilon(\tilde{\boldsymbol{X}})$ function corresponding to the Ψ function defined as the LPRE [35].

Back to the main problem of minimising $\boldsymbol{J}(\boldsymbol{X}, \boldsymbol{\Phi})$, assume that we have the dual functions $\Psi(\cdot)$ and $\Upsilon(\cdot)$. In [35], the authors proposed an algorithm that converges to a minimal point of $\boldsymbol{J}(\boldsymbol{X}, \boldsymbol{\Phi})$, if at least one exists. The pseudo-code for this algorithm is given as follows:

- *Aim*: Clustering data according to the given model.
- *Inputs*:
  Appropriate distance function Ψ and its dual Υ.
  Set of realisations $\boldsymbol{X} = \{\mathbf{x}_1, \ldots, \mathbf{x}_n\}$.
  Number of clusters $\mathbf{C}$.
  Fuzzyness m.
  Halting threshold δ.
- *Output*:
  Fuzzy membership values p_{ij}, $1 \le i \le n$, $1 \le j \le C$.
  $\mathbf{C}$ cluster descriptors $\phi_1, \ldots, \phi_C$.
- *Method*:
  1 $l = 0$.
  2 Randomise $\phi_1, \ldots, \phi_C$.
  3 $l = l + 1$.
  4 Compute distances as $D_{ij} = \Psi(\mathbf{x}_i, \phi_j)$.
  5 Compute fuzzy membership values as equation (6).
  6 Store the fuzzification scheme as $p_{ij} = F_{lji}$.
  7 Renew clusters as (7).
  8 if $l > 1$ compute δ_l as (9).
  9 if $l = 1$ then go to 3, else if $\delta_l > \delta$ then go to 3 else return.

As shown in the preceding pseudo-code for the algorithm, the first step is to randomise a set of initial cluster descriptors $\phi_1, \ldots, \phi_C$. Then, for all $i = 1, \ldots, n$ and $j = 1, \ldots, C$ the distance from $\mathbf{x}_i$ to the jth cluster is computed as $(D_{ij} = \Psi(\mathbf{x}_i, \phi_j))$. As proved in [35], the p_{ij} should guide $\boldsymbol{J}(\boldsymbol{X}, \boldsymbol{\Phi})$ to reach its minimum point by

$$p_{ij} = \frac{D_{ij}^{-\frac{1}{m-1}}}{\sum_{k=1}^{c} D_{ik}^{-\frac{1}{m-1}}} \tag{6}$$

Then, each cluster should be rearranged to best fit the renewed fuzzy set.

$$\phi_j = \Upsilon\left(\{(\mathbf{x}_i, p_{ij}^m) | i = 1, \ldots, n\}\right) \tag{7}$$

This process iterates between finding D_{ij}, computing p_{ij} and rearranging the clusters, until its convergence.

The halting condition of the algorithm is the stationarity of the fuzzy membership maps. Assume that the algorithm has passed through one iteration. Also, assume that F_{ijk} is

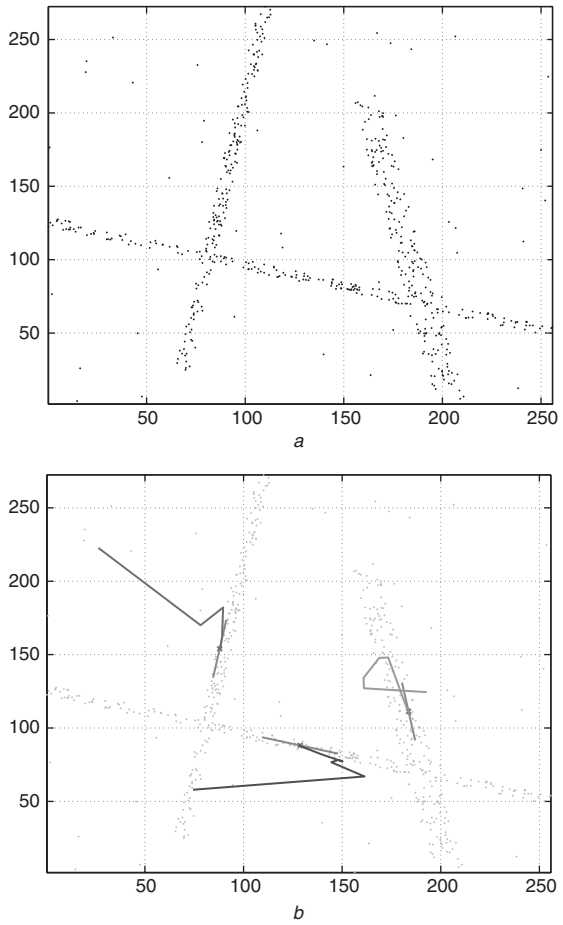

Fig. 2 *Results of applying the proposed clustering method on an artificial 2-D data cloud using the LPRE distance*
a Input data
b Resulted clusters and the path of clusters for convergence

the membership of $\mathbf{x}_k$ to the jth cluster in the ith iteration. Now, the difference between the result of the ith iteration and the jth iteration is defined as

$$\delta_{ij} = \sqrt{\frac{1}{WHc}\sum_{k=1}^{n}\sum_{l=1}^{C}(F_{ilk} - F_{jlk})^2} \tag{8}$$

Also, the repeatedness of the result of the lth iteration is defined as

$$\delta_l = \min\{\delta_{l,1}, \ldots, \delta_{l,l-1}\} \tag{9}$$

Now, the condition for ending the iterations is $\delta_i < \delta$, where δ is a predefined threshold. In this paper, we use $\delta = 0.05$; which means that the algorithm will stop iterating when the fuzzy membership values repeat with less than 5% variation.

Along with the FCM [29], other clustering approaches like Gustafson–Kessel (GK) [39], fuzzy elliptotypes clustering (FEC) [40] and fuzzy C-varieties (FCV) [41], are also special cases of the proposed general clustering method. See [35] for further details and mathematical discussions. Figure 2 illustrates a sample run on artificial 2D data using the LPRE distance.

Using the clustering procedure proposed in this paper with the LPRE methodology, a colour clustering tool is produced [35]. It must be emphasised that this formulation results in a special case of the FCV ($r = 1$) [40]. We call this method fuzzy principal-component analysis-based clustering (FPCAC).

When feeding an image $\mathbf{I}$ into the FPCAC process (with preselected values for C and m), the result is a set of C fuzzy maps $\mathbf{J}_1, \ldots, \mathbf{J}_C$. Here $\mathbf{J}_{ixy}$ denotes the level of membership of $\vec{\mathbf{I}}_{xy}$ to the ith cluster. Note that,

$$\forall_{x,y,} \sum_{i=1}^{C} \mathbf{J}_{ixy} = 1 \tag{10}$$

Fig. 3 *Results of the FPCAC method on some sample images*
a, *b*, *c*, *d* Original images
e, *f*, *g*, *h* Results of FPCAC
a and *b* Courtesy of Kodak PhotoCD (PCD0992)
c Courtesy of Ohio State University
d Lena, Courtesy of Singal and Image Processing Institute at University of Southern California.

In this paper, we change the fuzzy maps $\mathbf{J}_1, \ldots, \mathbf{J}_C$ into binary (crisp) maps $\bar{\mathbf{J}}_1, \ldots, \bar{\mathbf{J}}_C$ using maximum likelihood. As such,

$$\bar{\mathbf{J}}_{ixy} = \begin{cases} 1 & \forall j \neq i,\ \mathbf{J}_{jxy} < \mathbf{J}_{ixy} \\ 1 & \forall j < i,\ \mathbf{J}_{jxy} < \mathbf{J}_{ixy}\ \&\ \forall j > i,\ \mathbf{J}_{jxy} \leq \mathbf{J}_{ixy} \\ 0 & \text{otherwise.} \end{cases} \quad (11)$$

The complexity in definition of (11) is to compensate for the cases that, for a single pair of x and y, there are distinct values of i and j, for which $\mathbf{J}_{ixy} = \mathbf{J}_{jxy}$. As in this paper the binary FPCAC is utilised, we assume that the membership maps are binary ones, without emphasising that a maximum likelihood has passed over them. Figure 3 shows some examples for applying the FPCAC method on some sample images. These results are produced using $m = 1.2$ with values of $C = 3, 4, 3, 2$. The algorithm has converged in 14, 11, 12 and 9 successive iterations, elapsing 5.4, 5.5, 4.2 and 1.9 seconds, respectively.

2.4 Colour image recolouring

Assume that we have two homogeneous swatches of S_1 and S_2. Also, assume that $\boldsymbol{\eta}_1$, $\boldsymbol{\eta}_2$, $\mathbf{V}_1$ and $\mathbf{V}_2$ denote the expectation vectors and PCA (or FPCA) matrices of S_1 and S_2, respectively. Now, compute the vector $\boldsymbol{c}_2$, for the arbitrary vector $\boldsymbol{c}_1$ in S_1, as

$$\boldsymbol{c}_2 = \mathbf{V}_2\mathbf{V}_1^T(\boldsymbol{c}_1 - \boldsymbol{\eta}_1) + \boldsymbol{\eta}_2 \quad (12)$$

The vector $\boldsymbol{c}_2$ is the recolourised version of $\boldsymbol{c}_1$ according to the reference swatch of $\boldsymbol{C}_2$. Having $\boldsymbol{c}_2$, the vector $\boldsymbol{c}_1$ is reconstructed as

$$\boldsymbol{c}_1 = \mathbf{V}_1\mathbf{V}_2^T(\boldsymbol{c}_2 - \boldsymbol{\eta}_2) + \boldsymbol{\eta}_1 \quad (13)$$

This scheme is the PCA-based single-swatch recolouring process introduced in [30].

Figure 4 illustrates a sample result of this method. Figures 4*a* and 4*b* show the source and the reference images, respectively. Both images contain two homogeneous swatches which are given by the user to guide the recolouring process. Figures 4*c* and 4*d* illustrate the fuzzy membership maps of the source image according to these two swatches. Figures 4*e* and 4*f* show the single-swatch recolouring results and Fig. 4*g* shows the final result of the recolouring process. The total time elapsed on producing this result is 1.8 s. Note the high quality of the resulting image along with its low computational cost. Also, note the naturalistic contact of the sky and grasses at the horizon. In

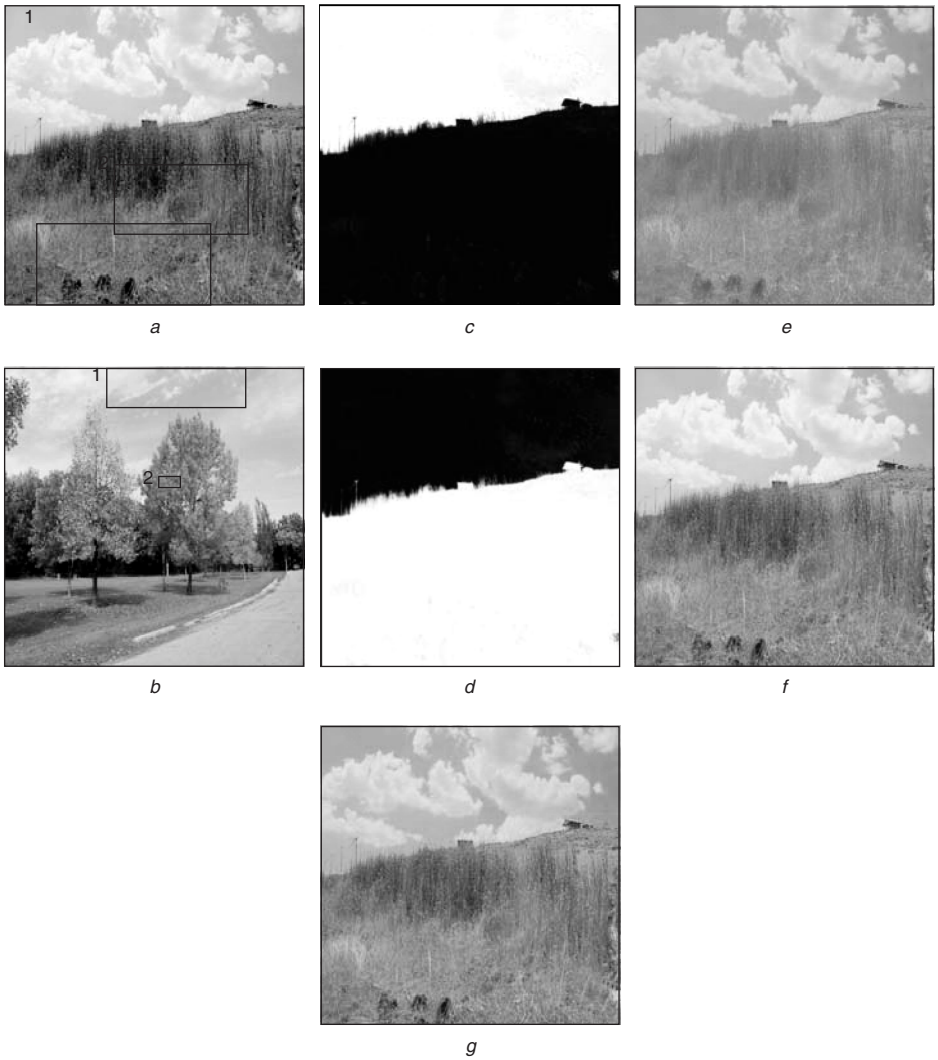

Fig. 4 *Illustrative sample for PCA-based recolouring*
a Source image
b Reference image
c and *d* Fuzzy membership maps
e and *f* Results of single-swatch recolouring
g Final result

this paper, we only use the single-swatch recolouring results shown in Figs. 4*e* and 4*f*.

2.5 Polarisation and depolarisation

There is a manipulated form of the common Euler angles that relates any right-rotating orthonormal matrix (such as V_{ij}) with three angles, in a one-to-one revertible transform [42].

A right-rotating orthonormal matrix is an orthonormal matrix which satisfies $(\mathbf{v}_1 \times \mathbf{v}_2) \cdot \mathbf{v}_3 > 0$, where $\times$ and $\cdot$ represent outer and inner products, respectively. Here, $\mathbf{v}_i$ is the ith column of $\mathbf{V}$. As such, for the right-rotating othonormal matrix $\mathbf{V}$, we write $\mathbf{V} \sim (\theta, \phi, \psi)$, when

$$\theta = \angle\left(\mathbf{v}_1^{xy}, [1, 0]^T\right) \tag{14}$$

$$\phi = \angle\left((\mathbf{R}_0^{xy}\mathbf{v}_1)^{xz}, [1, 0]^T\right) \tag{15}$$

$$\psi = \angle\left((\mathbf{R}_\phi^{xz}\mathbf{R}_0^{xy}\mathbf{v}_2)^{yz}, [1, 0]^T\right) \tag{16}$$

Here, $\angle(\mathbf{v}, \mathbf{u})$ denotes the angle between two vectors $\mathbf{v}, \mathbf{u} \in \mathbf{R}^2$, computed as

$$\angle(\mathbf{v}, \mathbf{u}) = \mathrm{sgn}((\mathbf{v} \times \mathbf{u}) \cdot j) \cos^{-1} \frac{\mathbf{v} \cdot \mathbf{u}}{\|\mathbf{v}\| \|\mathbf{u}\|}, \tag{17}$$

where $\mathrm{sgn}(x)$ is the signum function, defined as

$$\mathrm{sgn}(x) = \begin{cases} 1, & x > 0 \\ 0, & x = 0 \\ -1, & x < 0 \end{cases} \tag{18}$$

In (14)–(16), $\mathbf{v}_p$ denotes the project of the vector $\mathbf{v}$ on the plane p. Also, $\mathbf{R}_\alpha^p$ is the 3×3 matrix of α radians counterclockwise rotated in the p plane:

$$\mathbf{R}_\theta^{xy} = \begin{pmatrix} \cos\theta & -\sin\theta & 0 \\ \sin\theta & \cos\theta & 0 \\ 0 & 0 & 1 \end{pmatrix} \tag{19}$$

$$\mathbf{R}_\phi^{xz} = \begin{pmatrix} \cos\phi & 0 & -\sin\phi \\ 0 & 1 & 0 \\ \sin\phi & 0 & \cos\phi \end{pmatrix} \tag{20}$$

$$\mathbf{R}_\psi^{yz} = \begin{pmatrix} 0 & \cos\psi & -\sin\psi \\ 1 & 0 & 0 \\ 0 & \sin\psi & \cos\psi \end{pmatrix} \tag{21}$$

We can prove that

$$\mathbf{R}_\psi^{yz}\mathbf{R}_\phi^{xz}\mathbf{R}_\theta^{xy}\mathbf{V} = \mathbf{I} \tag{22}$$

Hence, to produce $\mathbf{V}$ out of the triple (θ, ϕ, ψ), we may use

$$\mathbf{V} = \mathbf{R}_{-\theta}^{xy}\mathbf{R}_{-\phi}^{xz}\mathbf{R}_{-\psi}^{yz} \tag{23}$$

Note that $(\mathbf{R}_\alpha^p)^{-1} = \mathbf{R}_{-\alpha}^p$. Then, while equations (14)–(16) compute the three angles θ, ϕ and ψ out of $\mathbf{V}$, equation (23) reconstructs $\mathbf{V}$ from θ, ϕ and ψ. These methods are called polarisation and depolarisation of a right-rotating orthonormal matrix, respectively [42].

2.6 Colour image copy protection

Figure 5 shows the flowchart of the proposed visual encryption/decryption method. Here, for the given image $\mathbf{I}_o$, the encryption block produces the encrypted demonstration image $\tilde{\mathbf{I}}$. It is done in a manner that $\tilde{\mathbf{I}}$ visualises the contents of $\mathbf{I}_o$ while containing deliberately embedded distortions that prevent an unauthorised consumer to use it for professional applications. When the authorisation is performed, the key $\mathbf{K}$ is given to the user. Using $\mathbf{K}$ and $\tilde{\mathbf{I}}$, the image $\mathbf{I}$ is reconstructed so that it perfectly duplicates

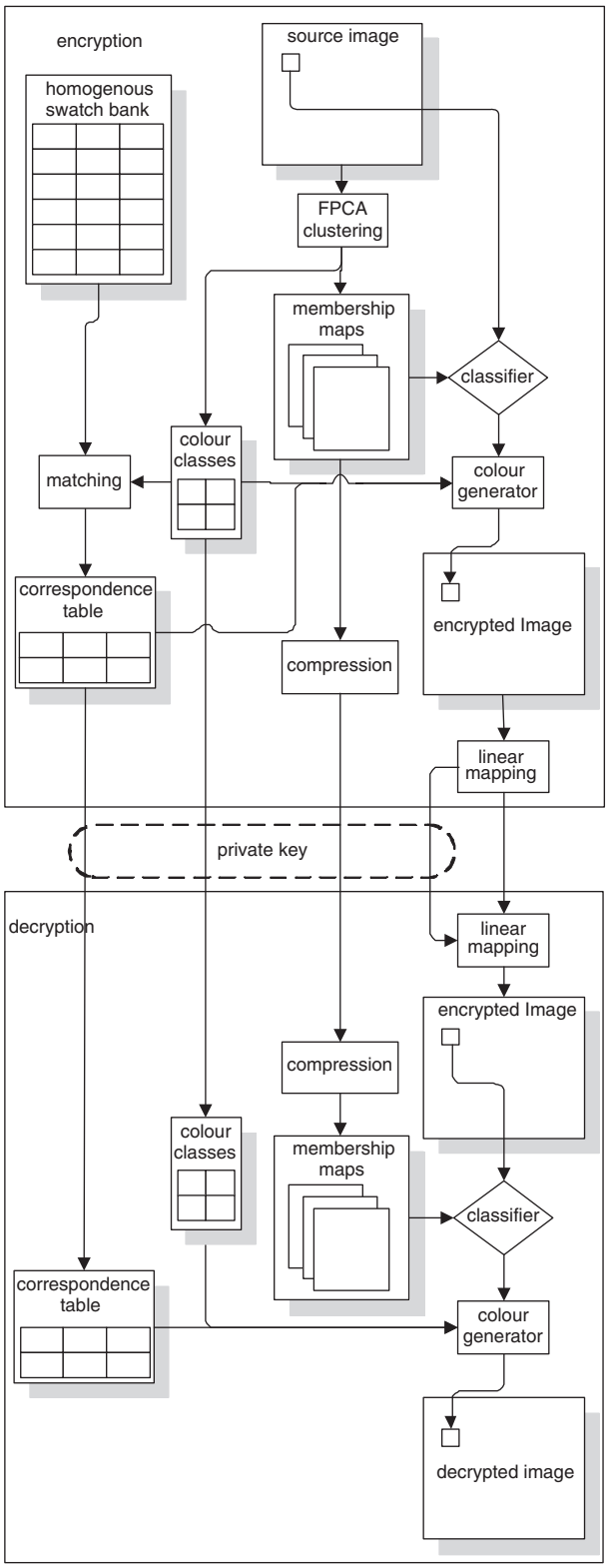

Fig. 5 *Flowchart of the proposed copy protection algorithm*

the original image $\mathbf{I}_o$. The main contributions of the proposed method are its robust protection against unauthorised duplication and distribution, the low elapsed time for encryption/decryption, high quality of the reconstructed image and the low redundancy of $\mathbf{K}$ over $\mathbf{I}_o$.

Assume that the original $H \times W$ image $\mathbf{I}_o$ is to be encrypted by the proposed method. As shown in Fig. 5, the FPCA clustering method is performed on $\mathbf{I}_o$. The results are a set of C colour classes $\phi_i = [\boldsymbol{\eta}_i, \mathbf{V}_i]$ for $i = 1, \ldots, C$ along with C, $H \times W$ binary membership maps $\mathbf{J}_1, \ldots, \mathbf{J}_C$. For

each value of i, the vector $\boldsymbol{\eta}_i$ is the fuzzy expectation vector of the colour vectors in the ith cluster [35]. Also, the $\mathbf{V}_i$ is the FPCA matrix of the ith cluster [35].

The FPCAC process depends on the fuzziness parameter (m) with default value of 1.05 for natural colour images [35]. As here we do not expect a satisfactory classification (in fact, we prefer some levels of degradation), the m value can be freely selected ($m > 1$). We propose to select m randomly using

$$m = 1 + |N(0, 1)| \tag{24}$$

where $N(0, 1)$ is a zero-mean unit-variance Gaussian random variable. In fact, m enables the proposed method to give any number of encrypted versions of a single image that are needed. Each encrypted image needs its own key to be unleashed. We will show this ability in Section 3.

Here, our main concern is a recolour a given image in an unsupervised manner, such that the image content remains understandable, while its quality degrades considerably. Thus, we propose a disturbing multi-swatch recolouring algorithm that is reversible. Assume producing the $H \times W$ index map $\mathbf{J}$ with its elements being members of $\{1, \ldots, C\}$. As such, $\mathbf{J}_{xy} = i$ if and only if $\mathbf{J}_{ixy} = 1$. As described in Section 2.3, there is one and only one choice for $\mathbf{J}$. Using the single-swatch recolouring method discussed in Section 2.4, we construct the encrypted image as

$$\tilde{\mathbf{I}}_{xy} = \mathbf{U}_i \mathbf{V}_i^T (\tilde{\mathbf{I}}_{oxy} - \boldsymbol{\eta}_i) + \boldsymbol{\rho}_i, i = J_{xy} \tag{25}$$

where $[\boldsymbol{\rho}_i, \mathbf{U}_i]$ for $i = 1, \ldots, C$ are a set of colour descriptors and x and y are image co-ordinates. We will return to these colour descriptors later. For now, it suffices to know that $\boldsymbol{\rho}_i$ is a 3×1 vector and $\mathbf{U}_i$ is a 3×3 unitary matrix.

In fact, in (25) each colour vector is transferred from the colour descriptor to which it mostly belongs to a second colour descriptor. Having $\mathbf{J}$ and $[\boldsymbol{\rho}_i, \mathbf{U}_i]$ for $i = 1, \ldots, C$, the original image is reconstructed from $\tilde{\mathbf{I}}$. Hence, $\mathbf{J}$ and $\{[\boldsymbol{\rho}_i, \mathbf{U}_i] | i = 1, \ldots, C\}$ produce the key ($\mathbf{K}$). The J is a large image and occupies memory, but, owing to its content, conventional lossless binary compression methods are highly efficient for compressing it. Furthermore, we propose to apply a convolution kernel of radius r on the membership map of the FPCAC, prior to the maximum likelihood process. This is done to produce an index map with more smoothed edges. This will result in an index map with a few holes and less isolated pixels (which declines the performance of the runlength coding).

Also, we propose to compute the redundancy of the key as its volume in compressed format over the volume of the whole image. Thus, the redundancy of the key $\mathbf{K}$ over the $H \times W$ image $\mathbf{I}_o$ is denoted by ε and is computed as

$$\varepsilon = \frac{\|\mathbf{K}\|}{\|\mathbf{I}\|} = \frac{\|\mathbf{K}\|}{3HW} \tag{26}$$

where $\|\mathbf{X}\|$ denotes the volume of $\mathbf{X}$ in bytes and $\mathbf{K}$ contains $[\boldsymbol{\rho}_i, \mathbf{U}_i]$ and $\mathbf{J}$.

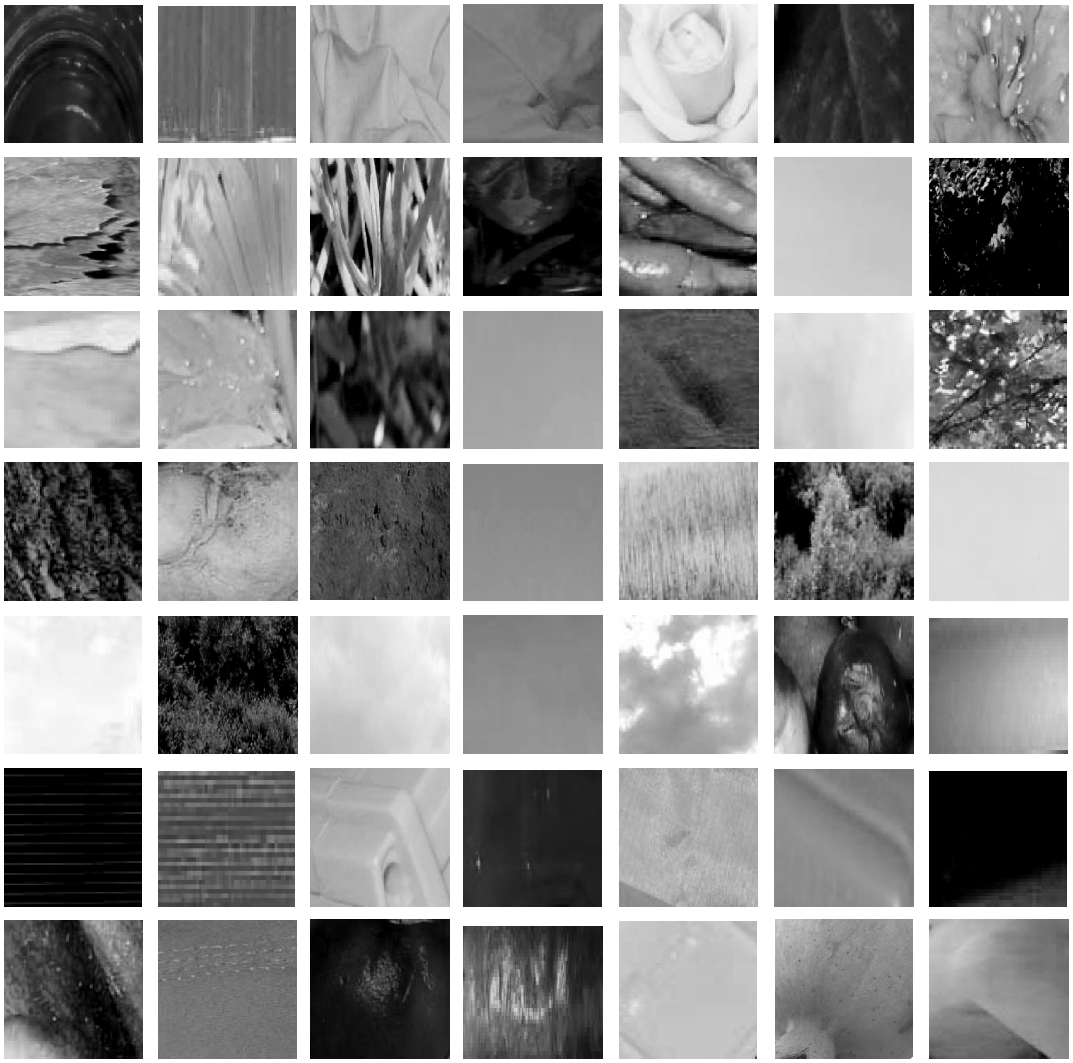

Fig. 6 *Homogeneous swatch bank*

One problem that arises here is that the $\tilde{\mathbf{I}}$ computed in (25) may contain values out of the range of [0, 255]. As the result of encryption is saved in one of the standard colour image formats (1 byte per pixel), these truncations produce artifacts in the results of decryption. Thus, we propose to apply a linear mapping on $\tilde{\mathbf{I}}$ and to send the parameters of the mapping, which are a bias and a scale, to the decryption stage.

The decryption process is performed in a straightly inverse fashion. Note that, theoretically, the process is completely reversible. We show (by examples) that, except for numerical errors, no information is lost during the encryption-decryption process.

Now, let us go back to the reference colour descriptors ($[\boldsymbol{\rho}_i, \mathbf{U}_i]$ for $i = 1, \ldots, C$). In fact, as the proposed visual encryption method is making fake edges, it is very important to alter the colour appearance of the image deliberately. We propose to use a bank of homogeneous swatches for this purpose (see Fig. 6). Assume that the bank contains k swatches with the colour descriptors of $[\boldsymbol{\rho}_i, \mathbf{U}_i]$ for $i = 1, \ldots, k$. The correspondence table in Fig. 5 holds an index to this bank for each cluster. The elements of this table are produced by a proposed matching process which compares two colour descriptors. The comparison is performed using a weighted Euclidean distance incorporating the expectation vectors and the polarised version of the PCA matrices discussed in Section 2.5.

Doing as such, the distance between a cluster of the image (with expectation vector of $\boldsymbol{\eta}$ and FPCA matrix of $\mathbf{V}$) and a homogeneous swatch in the bank (with expectation vector of $\boldsymbol{\rho}$ and PCA matrix of $\mathbf{U}$) is defined as

$$\delta^2 = \frac{1}{4\pi^2}\Big[(\theta_{\mathbf{V}} - \theta_{\mathbf{U}})^2 + (\phi_{\mathbf{V}} - \phi_{\mathbf{U}})^2 + (\psi_{\mathbf{V}} - \psi_{\mathbf{U}})^2\Big] + \frac{1}{255^2}\|\boldsymbol{\eta} - \boldsymbol{\eta}\|^2 \tag{27}$$

The $1/4\pi^2$ and $1/255^2$ coefficients are added to map both angles and colour values to the range [0, 1]. So, for each cluster, a proper homogeneous swatch is selected and its descriptor is used to encrypt the image and is also sent to the decryption process to decrypt the true colour vectors. The following Section is an experimental evaluation of the proposed method.

3 Experimental results

The proposed algorithm is developed in MATLAB 6.5, on a PIV 2600 MHz personal computer with 512 MB of RAM. In practice, WinZip 7.0 SR-1 (1285) by Nico Mark Computing Inc. is used as the compression process for the key.

Figure 6 shows the homogeneous swatch bank used in this work. The bank contains 49 swatches manually extracted from some colour images captured by an A60 Canon digital camera. The images are acquired from the natural and artificial objects in daylight or with flash. No other specific constraints are fulfilled. The colour descriptors of the swatches of the bank are saved in a .mat file occupying 6184 bytes of memory (in noncompressed format). After this stage, the swatches are not used and the extracted colour information is used.

Figure 7 shows some sample images used in this study. All these images are adopted from colour transfer literature. In different experiments, it is proved that the actual number of cluster of the FPCAC does not affect the performance of the algorithm. In this paper, we illustrate samples relating to the $C = 3$, but similar results are obtained for other vales of C. In fact, no user supervision is needed for determining the actual value of C. Note that the actual value of C is a secured parameter, which blocks cheating attempts. The radius of the convolution kernel in all experiments is set to 5. There are no other parameters in the proposed method to be selected by the user. Hence, the method is a fully unsupervised approach.

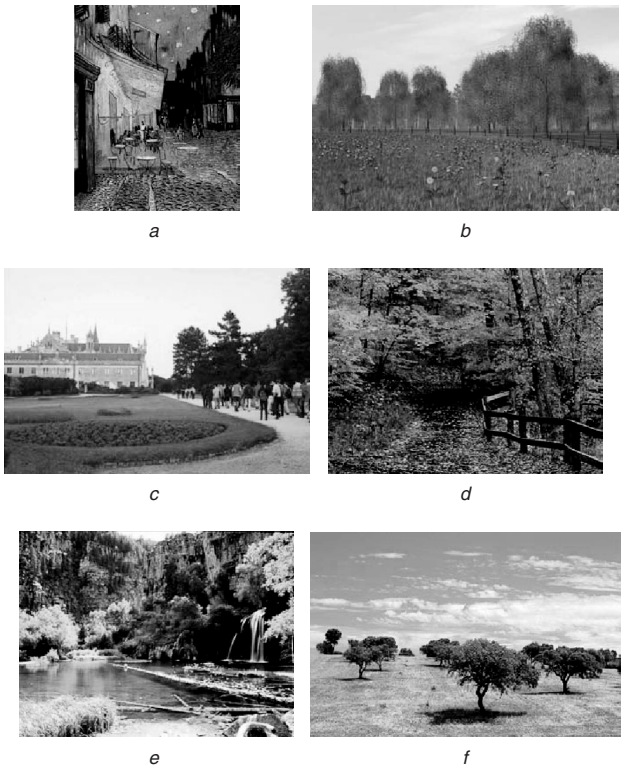

Fig. 7 *Some sample images*
a Vincent van Gogh's Cafe Terrace on the Place du Forum, Arles, at Night, Arles, September 1888, oil on canvas, image from the Vincent van Gogh Gallery, http://www.vangoghgallery.com
b and *c* Courtesy of Oliver Deussen
a, *b* and *c* adopted from [44]
d 'McCormic Creek State Park, Indiana' by Mike Briner, mbphoto@spraynet.com, www.mikebrinerphoto.com
e 'Hanging Lake' by Brent Reed, brent@reedservices.com
f Adopted from [45]

The proposed encryption/decryption process is performed on images shown in Fig. 7. The peak signal-to-noise ratio (PSNR) is computed between the original images and the decrypted images. Also, the redundancy of the key is computed. Two elapsed times are measured: t_1 is the time needed to encrypt an image and t_2 is the time needed to decrypt it. Numerical data are listed in Table 2. In

Table 2: Numerical results of proposed algorithm perfomed on images shown in Fig. 7

Image	Size	m	t_1 (s)	t_2 (s)	PSNR (dB)	ε (%)
7*a*	482 × 683	1.05	8.9	2.8	45.3	0.81
7*b*	896 × 602	1.05	14.9	5.2	46.6	0.60
7*c*	896 × 602	1.05	16.4	5.1	46.9	0.73
7*d*	600 × 450	1.05	8.2	2.6	45.7	1.69
7*e*	600 × 450	1.05	10.8	2.7	45.0	1.30
7*f*	680 × 448	1.05	8.8	3.0	45.2	0.73

m = fuzziness; t_1 = encryption time; t_2 = decryption time; PSNR after reconstructing the image; ε = redundancy of key

Fig. 8 *Encrypted versions of the images shown in Fig. 7, using proposed algorithm*

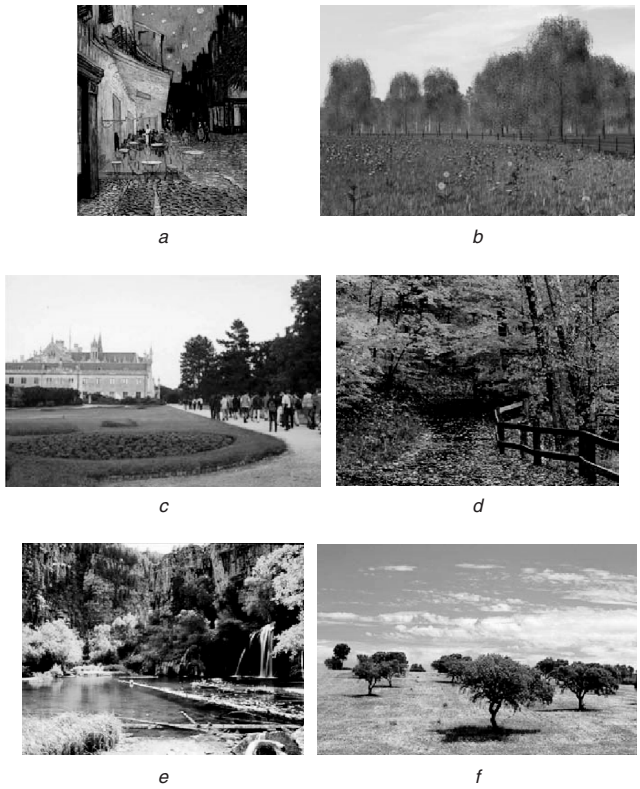

Fig. 9 *Decrypted versions of the images shown in Fig. 8 using proposed method*

this experiment, we have fixed the value of m equal to 1.05. It is observed in this experiment that, in all cases, the PSNR is above 45 dB. Note that, as indicated recently, PSNR values of above 38 dB are visually satisfactory even for

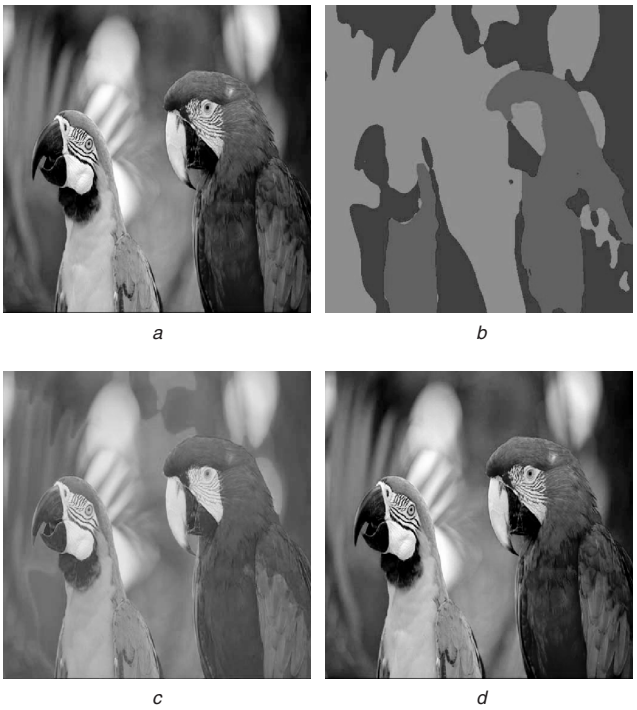

Fig. 10 *Sequential results of proposed algorithm*
a Original image, courtesy of Kodak PhotoCD (PCD0992)
b Results of FPCA clustering
c Encrypted image
d Decrypted image

professionals [43]. Figures 8 and 9 show the encrypted and decrypted images, respectively. Note the distorted pattern of edges in the pavement, sky and grass regions in Figs. 8*a*–8*c*. Also note that, in all encrypted images, while the content of the image is readable, it is made unrealistic and unsatisfactory for unauthorised distribution. And note the perfect quality of the reconstructed images in Fig. 9. None of the intentionally produced artifacts are visible in reconstructed images. Furthermore, the redundancy of the key is less than 2% in all cases, and the elapsed time for a set of encryption and decryption stages is 15 s on average (always less than 20 s). The interesting feature is that, on average 75% of the computational load is for the supplier, which can have specialised acceleration tools to boost the performance.

Figure 10 illustrates the sequential results of the proposed method. Figure 10*a* shows the original image, Fig. 10*b* shows the results of FPCA clustering and Fig. 10*c* shows the encrypted image, then Fig. 10*d* shows the results of decryption. In this example, $m = 1.29$ and we have $t_1 = 7.7$ s and $t_2 = 1.7$ s. The resulting PSNR is 45 dB and the redundancy of the key is less than 0.9%.

The important question here is the security of the proposed method. It is not enough to know m to infer the code of an image. This is based on an interesting feature of the FPCA clustering method. In fact, FPCAC is not a repeatable operation. This is theoretically trivial because FPCAC starts from an entirely random set of clusters. Figure 11 shows the results of nine runs of FPCAC on a single image with a unique set of parameters ($C = 3$, $m = 1.2$). Table 3 lists the mean square distance between different clustering results. This Table shows that there is, on average, 16% difference between the clustering results of the same image, compensated for switched clusters. Another interesting feature is that only three pairs are more than 95% alike (*a*–*e*, *b*–*i* and *f*–*g*). As such, in nine trials, six distinct clustering results are encountered. We

emphasise that here we have assumed that the attacker knows C and m, lacking knowledge of which makes cracking the code ultimately harder. Figure 12 shows nine different encryptions of a single image with different values of m.

Here, we examine a scenario for attacking the proposed encryption method. Assume that the attacker has an encrypted image and a key to a different encryption of that image, and wants to use the key in place. In the worst situation, assume that the two encryptions share the same values of C and m. Figure 13 illustrates this situation. With the desperate results of this experiment (switched code resulted in $PSNR < 12$ dB), the high security of the proposed method is clear. The reader should be aware that the difference between two distinct encryptions of a single image mainly relies on the different results of the FPCAC. Hence, in a practical system, having the history of encryption will help to avoid producing a similarly-repeated encryption. This will eventually result in maximum security of the proposed method.

We have not discussed the cracking attempt which depends on cheating the index map and the colour descriptors manually. We believe that, according to the complexity of producing an image-sized indexed map, this is a dead end. Also, note that as the edges of the index map are completely merged with the edges of the original image,

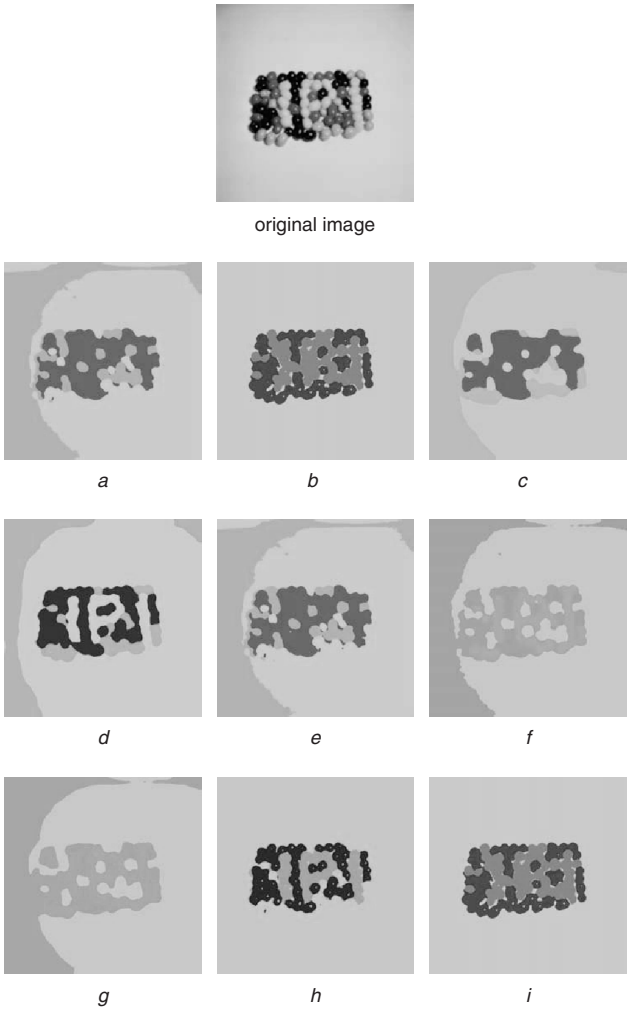

Fig. 11 *Results of applying FPCAC with a unique set of parameters on a single image for 9 different runs*
Original image, courtesy of Signal and Image Processing Institute at University of Southern California

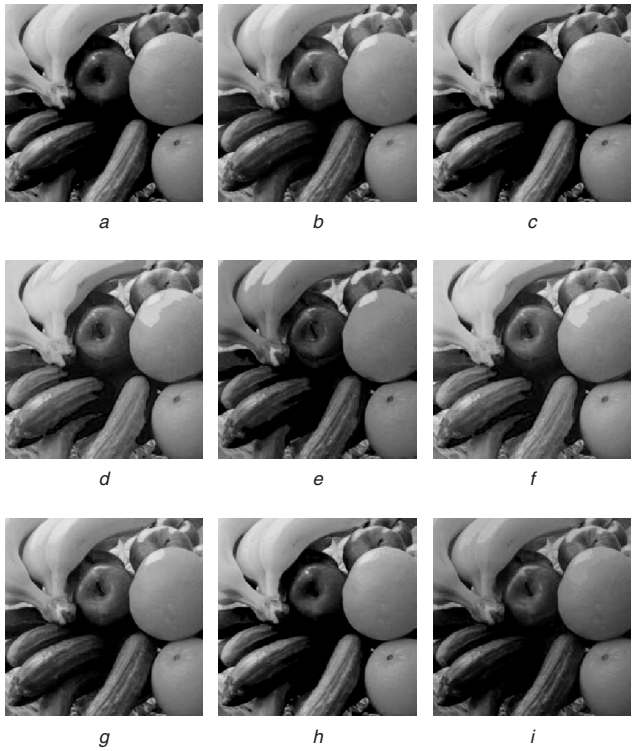

Fig. 12 *Different encryptions of a single image*

Table 3: Mean square distance between different clustering results of a single image with a unique set of parameters

Trial	*a*	*b*	*c*	*d*	*e*	*f*	*g*	*h*	*i*
a	0	0.23	0.091	0.17	**0.0042**	0.14	0.12	0.21	0.23
b	0.23	0	0.23	0.17	0.23	0.21	0.23	0.059	**0.00063**
c	0.091	0.23	0	0.12	0.093	0.086	0.088	0.25	0.23
d	0.17	0.17	0.12	0	0.17	0.19	0.2	0.17	0.17
e	**0.0042**	0.23	0.093	0.17	0	0.14	0.13	0.21	0.23
f	0.14	0.21	0.086	0.19	0.14	0	**0.024**	0.22	0.21
g	0.12	0.23	0.088	0.2	0.13	**0.024**	0	0.23	0.23
h	0.21	0.059	0.25	0.17	0.21	0.22	0.23	0	0.059
i	0.23	**0.00063**	0.23	0.17	0.23	0.21	0.23	0.059	0

Values less than 0.05 are written in bold. Images are shown in Fig. 11

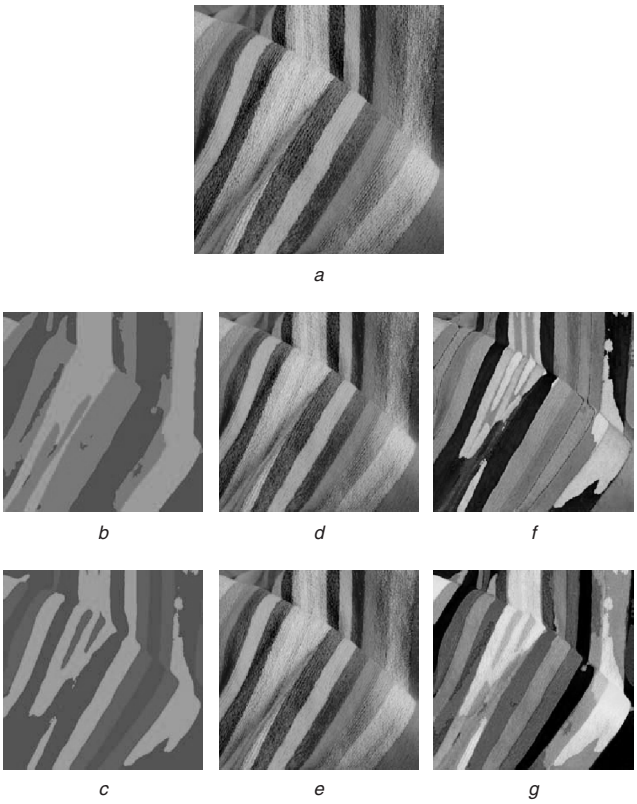

Fig. 13 *Decryption an image with an invalid key when C and m are known*
a Original image
b and *c* Results of FPCAC
d and *e* Decryption with correct keys
f and *g* Decryption with invalid (switched) keys

it is impractical to even re-engineer the index map by manual efforts.

4 Conclusions

With the recent developments in digital communications and the ease of access to multimedia resources, the need for protection against unauthorised duplication and distribution of digital media has arisen. In this paper, a novel and efficient unsupervised colour-image copy-protection method is proposed and analysed. In contrast with the commonly-used watermarking approaches that embed the owner authentication data into the original data, the proposed method applies reversible deliberate distortions in the original image. This method permits the efficient reconstruction of the original from and evaluation image which is not appropriate for professional distribution. Furthermore, while almost all of the available watermarking methods are not resistant to obvious attack, the proposed method prevents unauthorised distribution and gives a higher confidence to true ownership of digital media. The method is also fast and reliable.

5 Acknowledgment

This work was in part supported by a grant from ITRC. The authors wish to thank Dr. Gregory J. McGarry for his editorial comments. We also deeply appreciate the respected anonymous referees for their constructive suggestions. Arash Abadpour wishes to thank Ms. Azadeh Yadollahi for her encouragement and invaluable ideas.

6 References

1 Swanson, M., Kobayashi, M., and Twefik, A.: 'Multimedia data-embedding and watermarking technologies', *Proc. IEEE*, 1998, **86**, (6), pp. 1064–1087
2 Ruanaidh, J., Dowling, W., and Boland, F.: 'Watermarking digital images for copyright protection', *IEE Proc. Vis. Image Signal Process.*, 1996, **143**, (4), pp. 250–256
3 Kutter, M., Jordan, F., and Bossen, F.: 'Digital watermarking of color images using amplitude modulation', *Electron. Imaging*, 1998, **7**, (2), pp. 326–332
4 Yu, P.-T., Tasi, H.-H., and Lin, J.-S.: 'Digital watermarking based on neural networks for color images', *Signal Process.*, 2001, **81**, pp. 663–671
5 Chou, C.-H., and Wu, T.-L.: 'Embedding color watermarks in color images', *EURASIP J. Appl. Signal Process.*, 2001, **1**, pp. 327–332
6 Tsai, P., Hu, Y.-C., and Chang, C.-C.: 'A color image watermarking scheme based on color quantization', *Signal Process.*, 2004, **84**, pp. 95–106
7 Chung, T.-Y., Hong, M.-S., Oh, Y.-N., Shin, D.-H., and Park, S.-H.: 'Digital watermarking for copyright protection mpeg2 compressed video', *IEEE Trans. Consum. Electron.*, 1998, **44**, (3), pp. 895–901
8 Busch, C., Funk, W., and Wolthusen, S.: 'Digital watermarking: From concepts to real-time video applications', *IEEE Comput. Graph. Appl.*, 1999, pp. 25–35
9 Bloom, J.A., Cox, I.J., Kalker, T., Linnartz, J.-P.M.G., Miller, M.L., and Traw, C.B.S.: 'Copy protection for dvd video', *Proc. IEEE*, 1999, **87**, (7), pp. 1267–1276
10 Maes, M., Kalker, T., Linnartz, J.-P.M., Talstra, J., Depovere, G.F.G., and Haitsma, J.: 'Digital watermarking for dvd copy protection, what issues play a role in designing an effective system', *IEEE Signal Process. Mag.*, 2000, pp. 47–57
11 Langelaar, G.C., Setyawan, I., and Lagendijk, R.L.: 'Watermarking digital image and video data, a state-of-the-art overview', *IEEE Signal Process. Mag.*, 2000, pp. 20–46
12 Wu, C.W.: 'On the design of content-based multimedia authentication systems', *IEEE Trans. Multimed.*, 2002, **4**, (3), pp. 385–393
13 Mathai, N.J., Kundur, D., and Sheikholeslami, A.: 'Hardware implementation perspectives of digital video watermarking algorithms', *IEEE Trans. Signal Process.*, 2003, **51**, (4), pp. 625–638
14 Doerr, G., and Dugelay, J.-L.: 'A guide tour of video watermarking', *Signal Process., Image Commun.*, 2003, **18**, pp. 263–282
15 Kundur, D., and Marthik, K.: 'Video fingerprinting and encryption principles for digital rights management', *Proc. IEEE*, 2004, **92**, (6), pp. 918–932
16 Wallach, D.S.: 'Copy protection technology is doomed', *IEEE Computer*, 2001, **34**, (10), pp. 48–49
17 Kutter, M., and Petitcolas, F.A.P.: 'A fair benchmark for image watermarking systems'. Electronic Imaging'99 Security and Watermarking of Multimedia Content, San Jose, CA, USA, 1990, **3657**, pp. 219–239
18 Petitcolas, F.A.P., Anderson, R.J., and Kuhn, M.G.: 'Attacks on copyright marking systems' in Aucsmith, D. (Ed.): 'Information Hiding'. Proceedings of Second International Workshop, IH98, LNCS 1525 (Springer-Verlag, Portland, Oregon, USA, 1998), pp. 219–239
19 Petitcolas, F.A.P.: 'Watermarking schemes evaluation', *IEEE Signal Proc. Mag.*, 2000, **17**, (5), pp. 58–64
20 Petitcolas, F.A.P.: 'Stirmark benchmark 4.0', http://www.peticolas.net/fabien/watermarking/evaluation/index.html (Visited 2004)
21 Craver, S.A., Wu, M., and Liu, B.: 'What can we reasonably expect from watermarks?'. IEEE Workshop on Application of Signal Processing to Audio and Acoustics, New Paltz, New York, 2001, pp. 223–226
22 Grisworld, B.: 'Stopping webway rubbery: On-line image protection in the digital age', bgriswol@pop2000.gsfc.nasa.goc (Visited 2004)
23 Herley, C.: 'Why watermarking is nonsense', *IEEE Signal Process. Mag.*, 2002, **19**, pp. 10–11
24 Moulin, P.: 'Comments on "why watermarking is nonsense"', *IEEE Signal Process. Mag.*, 2003, **20**, pp. 57–59
25 'What is the future for watermarking (part i)', *IEEE Signal Process. Mag.*, 2003, **20**, pp. 55–59
26 'What is the future for watermarking (part ii)', *IEEE Signal Process. Mag.*, 2003, **20**, pp. 53–57
27 Kim, C.: 'Content-based image copy detection', *Signal Process., Image Commun.*, 2003, **18**, pp. 169–184
28 Cheng, S.-C, and Hsia, S.-C.: 'Fast algorithm's for color image processing by principal component analysis', *J. Visual Commun. Image Representation*, 2003, **14**, pp. 184–203
29 Bezdek, J.C.: 'Pattern recognition with fuzzy objective function algorithms' (Plenum Press, New York, 1981)
30 Abadpour, A., and Kasaei, S.: 'A new fast fuzzy colour transfer method'. 4th IEEE Int. Signal Process. Inf. Technol. (ISSPIT 2004), Rome, Italy, 2004, pp. 72–75
31 Lucchese, L., and Mitra, S.: 'Colour segmentation based on separate anisotropic diffusion of chromatic and achromatic channels', *IEEE Proc. Vis. Image Signal Process.*, 2001, **148**, (3), pp. 141–150
32 Cheng, H., and Li, J.: 'Fuzzy homogeneity and scale-space approach to color image segmentation', *Pattern Recognit.*, 2003, **36**, pp. 1545–1562
33 Chaira, T., and Ray, A.: 'Fuzzy approach for color region extraction', *Pattern Recognit.*, 2003, **24**, pp. 1943–1950

34 Abadpour, A., and Kasaei, S.: 'A new parametric linear adaptive color space and its pca based implementation'. 9th Annu. CSI Comput. Conf. CSICC, Tehran, Iran, 2004, pp. 125–132
35 Abadpour, A., and Kasaei, S.: 'A fast and efficient fuzzy color transfer method'. 4th IEEE Int. Symp. Signal Process. Inf. Technol., Isspit, Rome, Italy, 2004, pp. 491–494
36 Abadpour, A., and Kasaei, S.: 'Performance analysis of three homogeneity criteria for color image processing'. IPM Workshop on Computer Vision, Tehran, Iran, 2004
37 Nikolaev, D.O., and Nikolayev, P.O.: 'Linear color segmentation and its implementation', *Computer Vis. Image Underst.*, 2004, **94**, pp. 115–139
38 Abadpour, A., and Kasaei, S.: 'New fast fuzzy method for query region extraction in color images'. 10th Annu. CSI Comput. Conf. (CSICC 2005), Tehran, Iran, 2005, pp. 53–59
39 Gustafson, D.E., and Kessel, W.C.: 'Fuzzy clustering with a fuzzy covariance matrix'. Proc. IEEE CDC, San Diego, CA, 1979, Vol. 2, pp. 761–766
40 Leski, J.M.: 'Fuzzy c-varieties/elliptotypes clustering in reproducing kernel hilbert space', *Fuzzy Sets Syst.*, 2004, **141**, pp. 259–280
41 Honda, K., Sugiura, N., and Ichihashi, H.: 'Robust local principal component analyser with fuzzy clustering'. IJCNN 2003 Conf. Proc., 2003, pp. 732–737
42 Abadpour, A., and Kasaei, S.: 'A new pca-based robust color image watermarking method'. 2nd IEEE Conf. Adv. Technol. GCC: Challenges and Solutions, Manama, Bahrain, 2004, pp. 326–331
43 Katzenbeisser, S., and Petitcolas, F.A.P.: 'Information hiding techniques for steganography and digital watermarking' (Artech House Inc., 2000)
44 Reinhard, E., Ashikhmin, M., Gooch, B., and Shirley, P.: 'Color transfer between images', *IEEE Comput. Graph. Appl.*, 2001, **21**, (5), pp. 34–41
45 Chang, Y., Saito, S., and Nakajima, M.: 'A framework for transfer colors based on the basic color categories'. IEEE Proc. Comput. Graph. Int., 2003, pp. 176–181
46 Nikoladis, A., and Pitas, I.: 'Robust watermarking of facial images based on salient geometric pattern matching', *IEEE Trans. Multimed.*, 2000, **2**, (3), pp. 172–184
47 Hsieh, M.-S., Tseng, D.-C., and Huang, Y.-H.: 'Hiding digital watermarks using multiresolution wavelet transform', *IEEE Trans. Ind. Electron.*, 2001, **48**, (5), pp. 875–882
48 Barni, M., Bartolini, F., and Piva, A.: 'Multichannel watermarking of color images', *IEEE Trans. Circuits Syst. Video Technol.*, 2002, **12**, (3), pp. 142–156
49 Kutter, M., and Winkler, S.: 'A vision-based masking model for spread-spectrum image watermarking', *IEEE Trans. Image Process.*, 2002, **11**, (1), pp. 16–25
50 Tang, C.-W., and Hang, H.-M.: 'A feature-based robust digital image watermarking scheme', *IEEE Trans. Signal Process.*, 2003, **51**, (4), pp. 950–959
51 Kang, X., Huang, J., Shi, Y.Q., and Lin, Y.: 'A dwt-dft composite watermarking scheme robust to both affine transform and jpeg compression', *IEEE Trans. Circuits Syst. Video Technol.*, 2003, **13**, (8), pp. 776–786
52 Hao, S., and Lin, Y.-P.: 'Wavelet tree quantization for copyright protection watermarking', *IEEE Trans. Image Process.*, 2004, **13**, (2), pp. 154–165